

AD-A145 782

IRREGULARITY DECAY IN AN ISOLATED PLASMA BUBBLE(U) SRI  
INTERNATIONAL MENLO PARK CA R C LIVINGSTON ET AL  
31 MAY 84 SCIENTIFIC-1 AFGL-TR-84-0146 F19628-84-K-0019

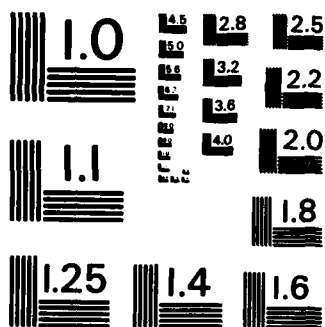
1/1

UNCLASSIFIED

F/G 4/1

NL





AFGL-TR-84-0146

AD-A145 782

12

IRREGULARITY DECAY IN AN  
ISOLATED PLASMA BUBBLE

R.C. Livingston  
J.F. Vickrey

SRI International  
333 Ravenswood Avenue  
Menlo Park, CA 94025

Scientific Report No. 1

31 May 1984

DTIC FILE COPY

Approved for public release; distribution unlimited

AIR FORCE GEOPHYSICS LABORATORY  
AIR FORCE SYSTEMS COMMAND  
UNITED STATES AIR FORCE  
HANSOM AFB, MASSACHUSETTS 01731

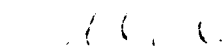
DTIC  
ELECTE  
SEP 21 1984  
S A D

9 09 21 011

This report has been reviewed by the ESD Public Affairs Office (PA) and is releasable to the National Information Service (NTIS).

"This technical report has been reviewed and is approved for publication."

FOR THE COMMANDER

  
\_\_\_\_\_  
Herbert C. Carlson, Jr.  
Branch Chief

  
\_\_\_\_\_  
Robert A. Skrivane, Director  
Division Director

Qualified requestors may obtain additional copies from the Defense Technical Information Center. All others should apply to the National Technical Information Service.

If your address has changed, or if you wish to be removed from the mailing list, or if the addressee is no longer employed by your organization, please notify AFGL/DAA, Hanscom AFB, MA 01731. This will assist us in maintaining a current mailing list.

UNCLASSIFIED

SECURITY CLASSIFICATION OF THIS PAGE

AD-A145782

## REPORT DOCUMENTATION PAGE

1a. REPORT SECURITY CLASSIFICATION <u>Unclassified</u>			1b. RESTRICTIVE MARKINGS None										
2a. SECURITY CLASSIFICATION AUTHORITY <u>N/A</u>			3. DISTRIBUTION/AVAILABILITY OF REPORT Approved for public release; Distribution unlimited										
2b. DECLASSIFICATION/DOWNGRADING SCHEDULE <u>N/A</u>													
4. PERFORMING ORGANIZATION REPORT NUMBER(S) SRI Project 5993			5. MONITORING ORGANIZATION REPORT NUMBER(S) AFGL-TR-84-0146										
6a. NAME OF PERFORMING ORGANIZATION SRI International		6b. OFFICE SYMBOL (If applicable) N/A		7a. NAME OF MONITORING ORGANIZATION Air Force Geophysics Laboratory (LIS)									
6c. ADDRESS (City, State and ZIP Code) 333 Ravenswood Avenue Menlo Park, CA 94025			7b. ADDRESS (City, State and ZIP Code) Hanscom Air Force Base Bedford, MA 01731										
8a. NAME OF FUNDING/SPONSORING ORGANIZATION AFGL		8b. OFFICE SYMBOL (If applicable) LIS		9. PROCUREMENT INSTRUMENT IDENTIFICATION NUMBER Contract No. F19628-84-K-0019									
8c. ADDRESS (City, State and ZIP Code) Hanscom Air Force Base Bedford, MA 01731 Monitor/Edward J. Weber			10. SOURCE OF FUNDING NOS. <table border="1"><tr><th>PROGRAM ELEMENT NO.</th><th>PROJECT NO.</th><th>TASK NO.</th><th>WORK UNIT NO.</th></tr><tr><td>62101F</td><td>4643</td><td>08</td><td>AE</td></tr></table>		PROGRAM ELEMENT NO.	PROJECT NO.	TASK NO.	WORK UNIT NO.	62101F	4643	08	AE	
PROGRAM ELEMENT NO.	PROJECT NO.	TASK NO.	WORK UNIT NO.										
62101F	4643	08	AE										
11. TITLE (Include Security Classification) Irregularity Decay in an Isolated Plasma Bubble (U)													
12. PERSONAL AUTHOR(S) R.C. Livingston and J.F. Vickrey													
13a. TYPE OF REPORT Scientific #1		13b. TIME COVERED FROM <u>10Oct83</u> TO <u>31May84</u>		14. DATE OF REPORT (Yr., Mo., Day) 31 May 1984									
15. PAGE COUNT 23													
16. SUPPLEMENTARY NOTATION													
17. COSATI CODES <table border="1"><tr><th>FIELD</th><th>GROUP</th><th>SUB. GR.</th></tr><tr><td>0401</td><td></td><td></td></tr><tr><td>2009</td><td></td><td></td></tr></table>			FIELD	GROUP	SUB. GR.	0401			2009			18. SUBJECT TERMS (Continue on reverse if necessary and identify by block number) F Region Irregularities Temporal Evolution Equatorial Spread F Phase Scintillation	
FIELD	GROUP	SUB. GR.											
0401													
2009													
19. ABSTRACT (Continue on reverse if necessary and identify by block number) Complex signal scintillation observations of an isolated and decaying equatorial plasma bubble are described. Multiple scans through the bubble made from the Air Force Geophysics Laboratory Airborne Ionospheric Observatory, show evolution of irregularity energy over a broad range of scale sizes. At wavelengths larger than about 4 km, the energy remains nearly constant with time. At shorter scale sizes, the spectrum maintains an approximate law form ( $f^{-n}$ ) and $n$ increases with time. This behavior suggests that the effective cross-field diffusion rate in the F region depends on scale size. Such a dependence has recently been predicted theoretically and is the result of magnetic field line coupling to the E layer.													
20. DISTRIBUTION/AVAILABILITY OF ABSTRACT UNCLASSIFIED/UNLIMITED <input checked="" type="checkbox"/> SAME AS RPT. <input type="checkbox"/> DTIC USERS <input type="checkbox"/>			21. ABSTRACT SECURITY CLASSIFICATION Unclassified										
22a. NAME OF RESPONSIBLE INDIVIDUAL Edward J. Weber			22b. TELEPHONE NUMBER (Include Area Code) 617-861-2131										
			22c. OFFICE SYMBOL AFGL/LIS										

# CONTENTS

LIST OF ILLUSTRATIONS . . . . .	iv
I INTRODUCTION . . . . .	1
II EXPERIMENT BACKGROUND . . . . .	2
III STRUCTURE OF TOTAL ELECTRON CONTENT AND INTENSITY SCINTILLATION . . . . .	5
IV PHASE SPECTRA AND IRREGULARITY DECAY . . . . .	9
V DISCUSSION . . . . .	15
A. Enhanced Classical Diffusion . . . . .	15
B. The Drift-Wave Hypothesis . . . . .	16
C. The Image Formation Process . . . . .	17
VI SUMMARY . . . . .	18
REFERENCES . . . . .	19



Accession For	
NTIS GRA&I	<input checked="" type="checkbox"/>
DTIC TAB	<input type="checkbox"/>
Unannounced	<input type="checkbox"/>
Justification	
By	
Distribution/	
Availability Codes	
Avail and/or	
Dist	Special
AI	

## LIST OF ILLUSTRATIONS

1	Map of the 350-km Altitude Ionospheric Penetration Point for Consecutive East-West Flight Legs . . . . .	3
2	6300-Å Airglow Images of the Bubble, with the Ionospheric Penetration Point Indicated . . . . .	4
3	Intensity and Phase Record for Scans through the Bubble . . . . .	6
4	One Possible Configuration of Electron Density (Contours) and Irregularity Distribution (Shaded) that Duplicates the Observed Signal Structures . . . . .	7
5	Phase Power Spectra for the Bubble . . . . .	10
6	Comparison of Observations of Theoretical Predictions Based on Eq. (1) . . . . .	13
7	Empirically Derived Diffusion Coefficient . . . . .	14

## I INTRODUCTION

Irregularity generation in the nighttime equatorial F region is dominated by the large-scale electron density structures that have come to be known as plasma bubbles. These depleted regions and the irregularities that they produce as they develop, are clearly associated with radar backscatter, ionogram spread F, airglow depletions and radio-wave scintillation [Ossakow, 1979, and references cited therein].\* Typically, the experimental effort has been directed toward understanding the growth and full-development phases of plasma bubbles in the early evening local-time sector. In this paper, we describe measurements of a much weaker, decay phase bubble. By making repeated scans through that bubble, detailed changes in its irregularity content have been measured.

The observations were made using the Air Force Geophysics Laboratory's (AFGL) Airborne Ionospheric Observatory. Previous measurements using the aircraft have established the bottomside airglow, spread-F and intensity scintillation signatures of equatorial plasma bubbles [e.g., Weber et al., 1980]. In early 1979, the scintillation measurement capability of the aircraft was expanded to record complex signal measurements from CW satellite sources using a technique outlined in Livingston [1983]. The phase of a transionospherically propagated signal is not strongly affected by diffraction at the frequencies and perturbation levels of interest here [Rino, 1979], and its power spectrum provides an almost direct mapping of the in situ irregularity continuum. The inherent sensitivity of the phase measurements also makes it possible to observe subtle changes in that continuum over a large range of spatial scales. This time/wavelength dependence of spectral energy is an essential element in the definition of irregularity decay.

---

\*The references are listed at the end of this report.



## II EXPERIMENT BACKGROUND

The observations included in this paper were made during a flight from Ascension Island on 27 and 28 March 1979; the objective of that flight was to locate an isolated, eastward-drifting plasma depletion, and to make repeated scintillation measurements through the disturbance as it decayed. A route was selected far enough south of the magnetic equator to ensure high enough background airglow intensities at 6300 Å to contrast with the plasma bubbles and associated airglow depletions. Early in the flight, one moderate airglow depletion was observed, but the structure had decayed before any propagation raypaths intersected the disturbance. A second depletion was encountered shortly thereafter, and at local times between 2300 to 0130 hours, a series of east-west legs were flown to make repeated scintillation and optical measurements of the bubble as it decayed.

Figure 1 is a map of the F-region (350-km) penetration point scanned by the aircraft during the multiple east-west flight legs. The successive tracks are nearly parallel, and each is at a constant dip latitude near  $13^{\circ}$ . The radio-scintillation source used throughout the scintillation measurements was a 249-MHz signal from a geostationary satellite located due west of the aircraft at an elevation of  $73^{\circ}$ . The aircraft speed was nearly constant in both eastward and westward directions producing a cross-field penetration velocity component of slightly greater than 200 m/s at F-region altitudes.

Figure 2 shows the all-sky 6300-Å airglow images for three times during the flight. The dots indicate the propagation-path intersection at the assumed airglow emission height of 250 km, where the all-sky lens images a circle of 600-km radius in the ionosphere. The airglow depletions visible in Figure 2, although structured, are relatively weak compared to others measured near Ascension Island in 1978 [Weber et al., 1980]. They do, however, verify that it is the same structure that is being intercepted on consecutive aircraft passes.

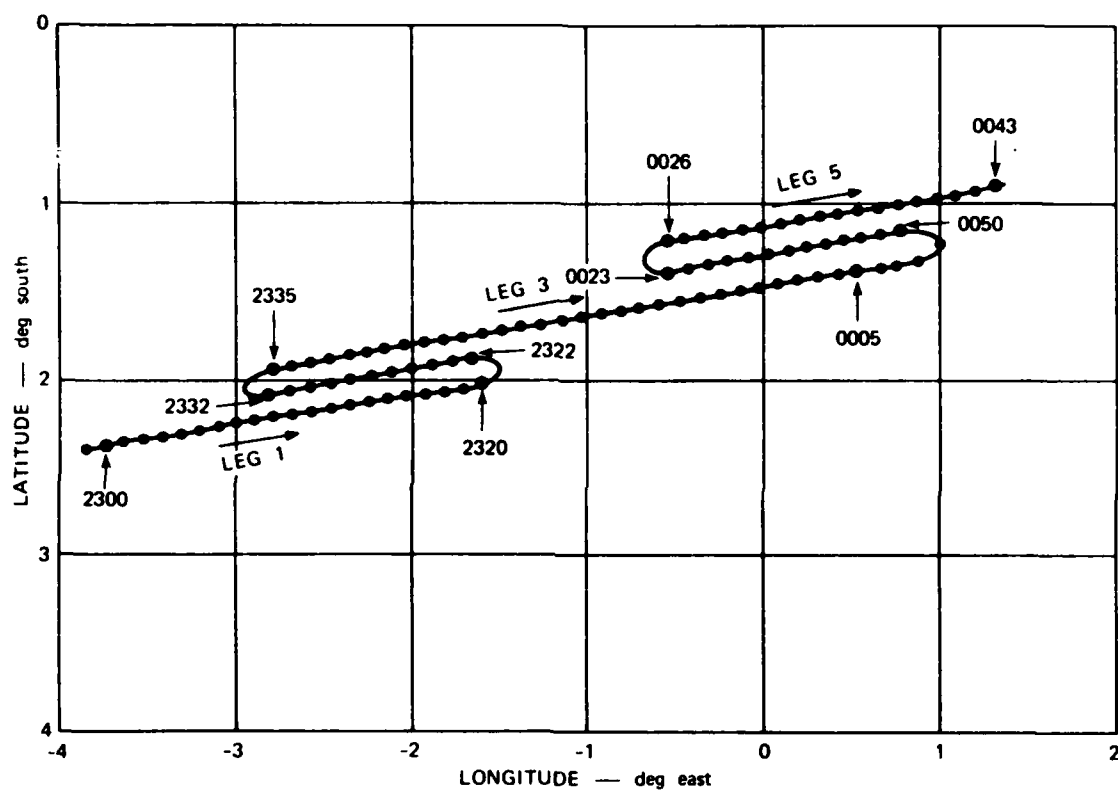


FIGURE 1 MAP OF THE 350-km ALTITUDE IONOSPHERIC PENETRATION POINT FOR CONSECUTIVE EAST-WEST FLIGHT LEGS

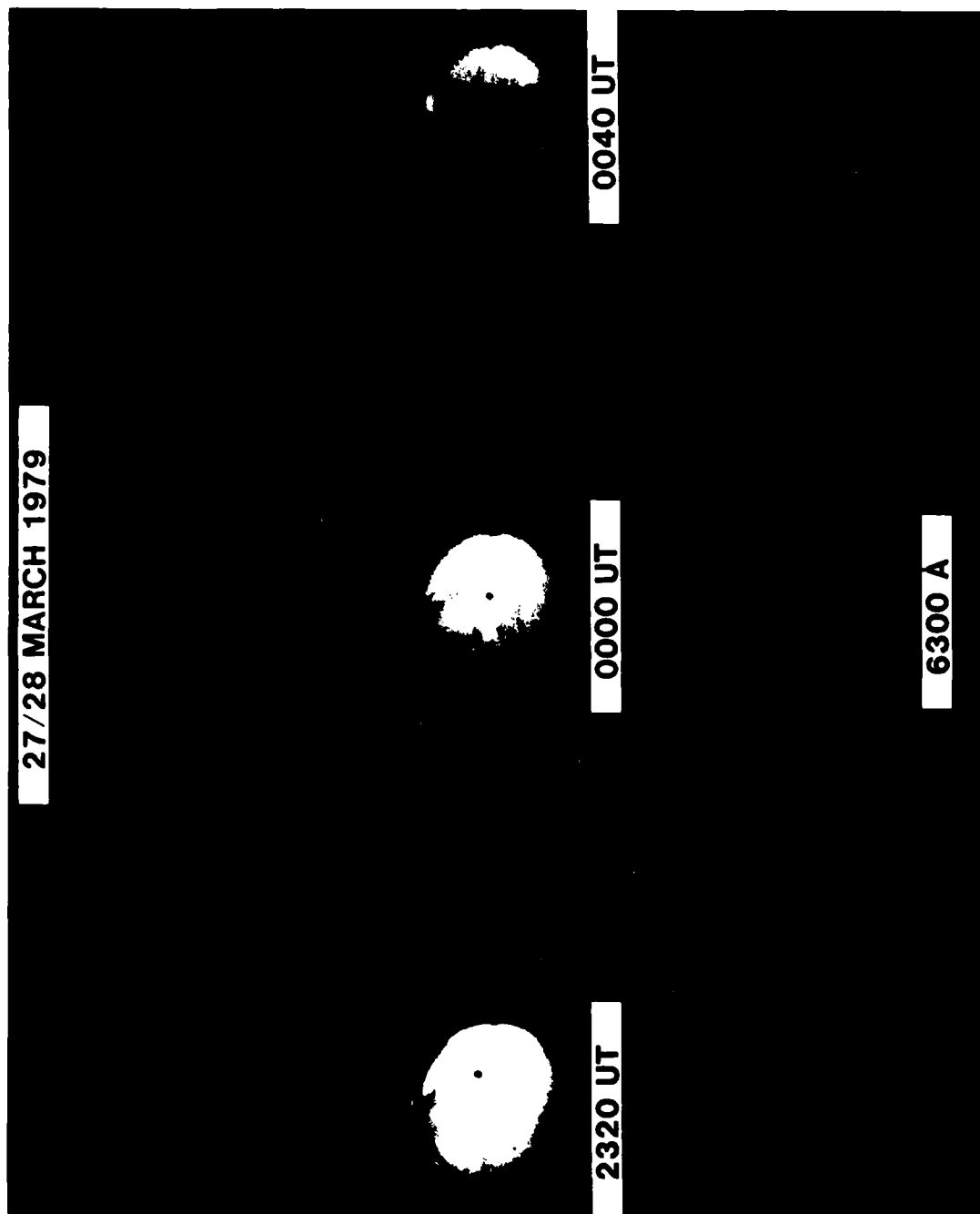


FIGURE 2 6300-Å AIRGLOW IMAGES OF THE BUBBLE, WITH THE IONOSPHERIC PENETRATION POINT INDICATED

### III STRUCTURE OF TOTAL ELECTRON CONTENT AND INTENSITY SCINTILLATION

Figure 3(a) shows the signal intensity and large-scale dispersive phase variation, flying eastward for Leg 1, the first scan through the bubble. The onset of intensity scintillation, which is caused by irregularities of  $\sim 200$ -m cross-field dimension, is very rapid on the western edge of the disturbance and is associated with a gradient in total electron content (TEC), which entails a decrease in column density of about  $1 \times 10^{17}$  electrons/m<sup>2</sup>.

The generation of plasma bubbles in the nighttime equatorial ionosphere is by now, a much-studied and reasonably well-understood process. In some cases, the bubble growth is moderate or stalls at an early stage, leaving a large, westward tilted density depletion in the bottomside F-region [Tsunoda, 1981]. Although the large-scale growth stage of the bubble itself has ended, its edges can structure as a result of the gradient drift instability. At these local times, the zonal neutral wind is large ( $\geq 150$  m/s) and eastward, so that westward-directed plasma gradients are unstable. Therefore, the westward edge of an upwelling is most likely to develop intermediate-scale structure. This behavior is consistent with Figure 4 which is a simple model based upon our  $\Delta$ TEC and scintillation data for Leg 1. The vertical extent of the bubble can only be guessed. There is no question, however, that the west wall is structured in regions where the plasma drift vector and the density gradients are parallel.

In Figures 3(b) through 3(e), the intensity scintillation and  $\Delta$ TEC for subsequent cuts through the drifting bubble are shown. For westward legs, the time scales have been reversed and expanded to match those eastward, in both direction and distance. The relative eastward/westward time scales were ascertained by first locating, in space (Figure 1), the westward intensity scintillation or depletion boundaries for consecutive legs. This yields a cross-field, macroscale drift of  $\sim 90$  m/s throughout the observation period at a penetration altitude of 350 km.

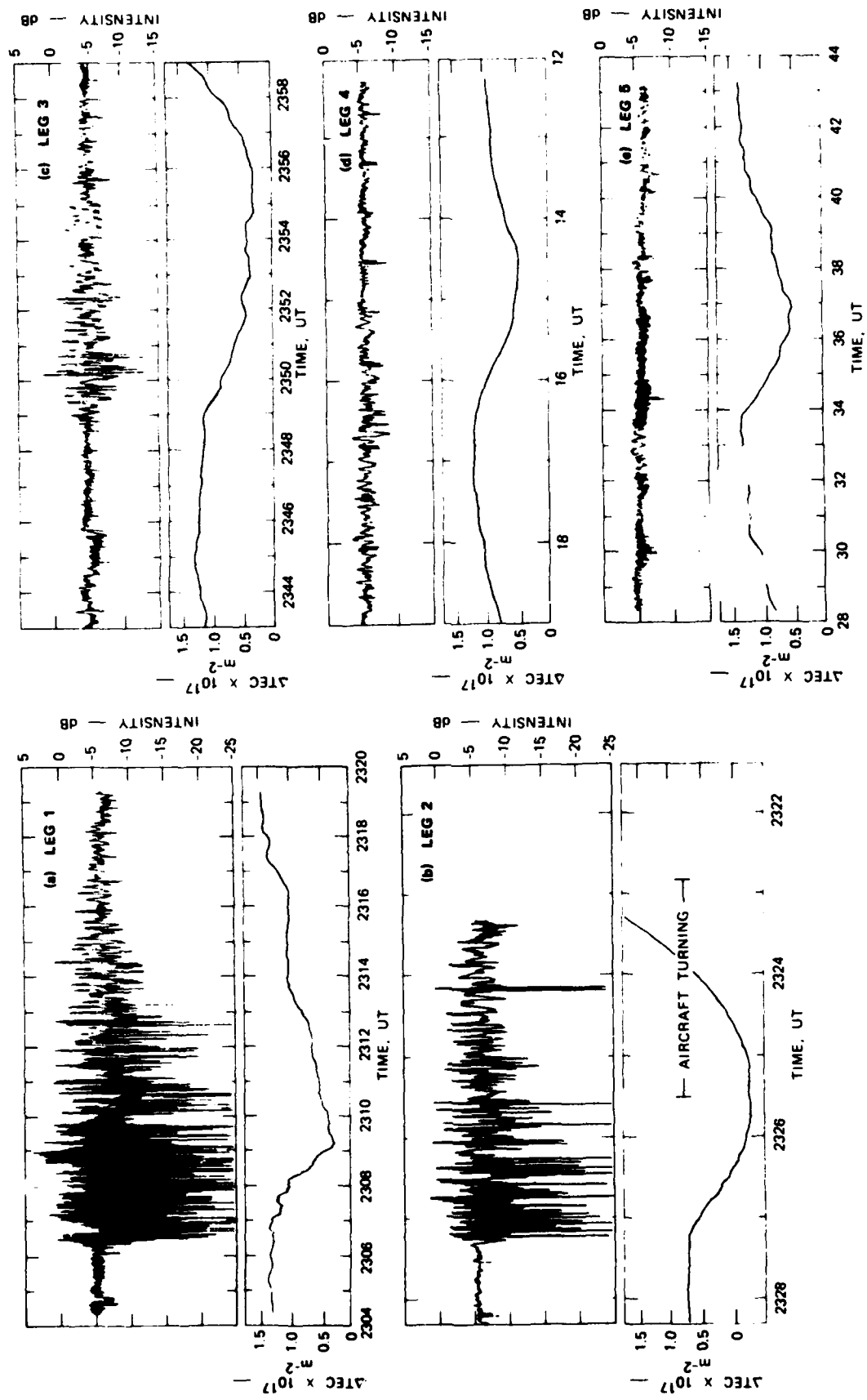


FIGURE 3 INTENSITY AND PHASE RECORDS FOR SCANS THROUGH THE BUBBLE

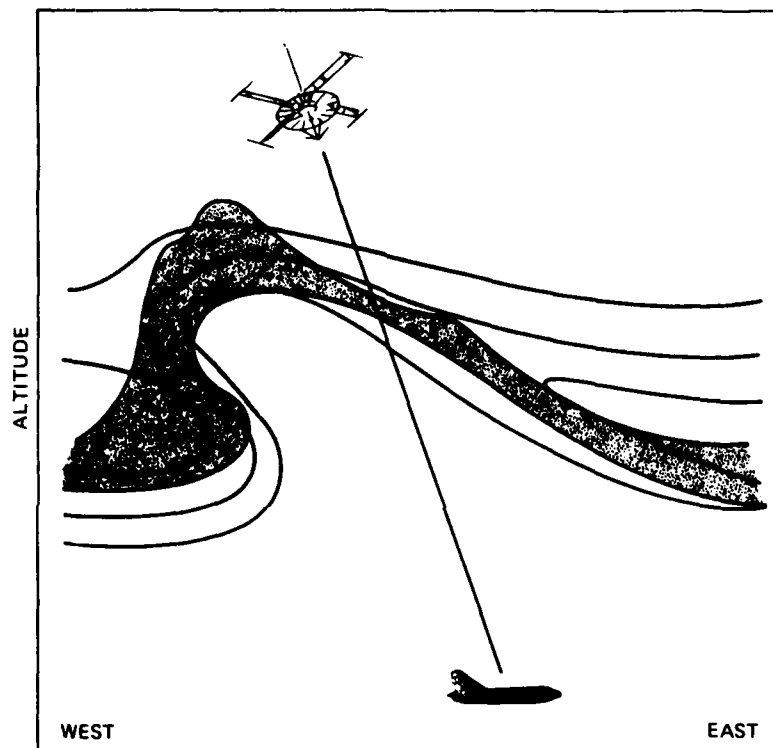


FIGURE 4 ONE POSSIBLE CONFIGURATION OF ELECTRON DENSITY (CONTOURS) AND IRREGULARITY DISTRIBUTION (SHADED) THAT DUPLICATES THE OBSERVED SIGNAL STRUCTURE

By comparing flight legs in Figure 3 it can be seen that the intensity scintillation declines rapidly to a level indistinguishable from the noise level by the fourth leg, but the  $\Delta$ TEC pattern remains nearly constant in form. (On the second leg, the phase data is distorted before 2325 UT by rapid aircraft deviation from straight and level flight.)

#### IV PHASE SPECTRA AND IRREGULARITY DECAY

The intensity records in Figure 3 effectively illustrate the east-west asymmetry in, and temporal decay of  $> 400$ -m spatial scale irregularities. The phase data and, in particular, the temporal changes in energy and the shape of the phase spectra from leg to leg, can be used to determine the decay rate quantitatively and provide information about possible decay mechanisms.

In Figure 5, the phase spectra of the overall bubble are shown for the three eastbound Legs (1, 3, and 5). These have been offset from one another by 10 dB for clarity. By including the entire bubble in each spectrum, we can observe structure in spatial wavelengths from the  $\sim 80$ -km outer scale down through about 400 m. For the eastbound flight, the bubble drifts with the aircraft, producing an effective scan rate of  $\sim 110$  m/s. This establishes the correspondence between the temporal and irregularity cross field spatial scales shown.

The spectrum for Leg 1 is in a familiar experimental form (although no theory has yet successfully predicted this power law index). It is nearly power law with an average spectral index near  $-2.5$ ; this slope and the spectral density levels agree well with those observed in morphological studies of irregularity spectra at the equator [e.g., Livingston et al., 1981]. Such a phase spectral index corresponds to a one-dimensional rocket or satellite spectrum with index of  $-1.5$ . We consider it, then, to be the signature of a region sampled during, or shortly after, Rayleigh-Taylor or gradient drift structuring or both, as already suggested. For Legs 3 and 5, however, sampled some 40 and 70 min after Leg 1, the spectra have considerably steepened through energy decay at short spatial scales. For purposes of discussion, we will use the break in the spectra, which this decay creates near 4 km, as the dividing line between two different regimes.



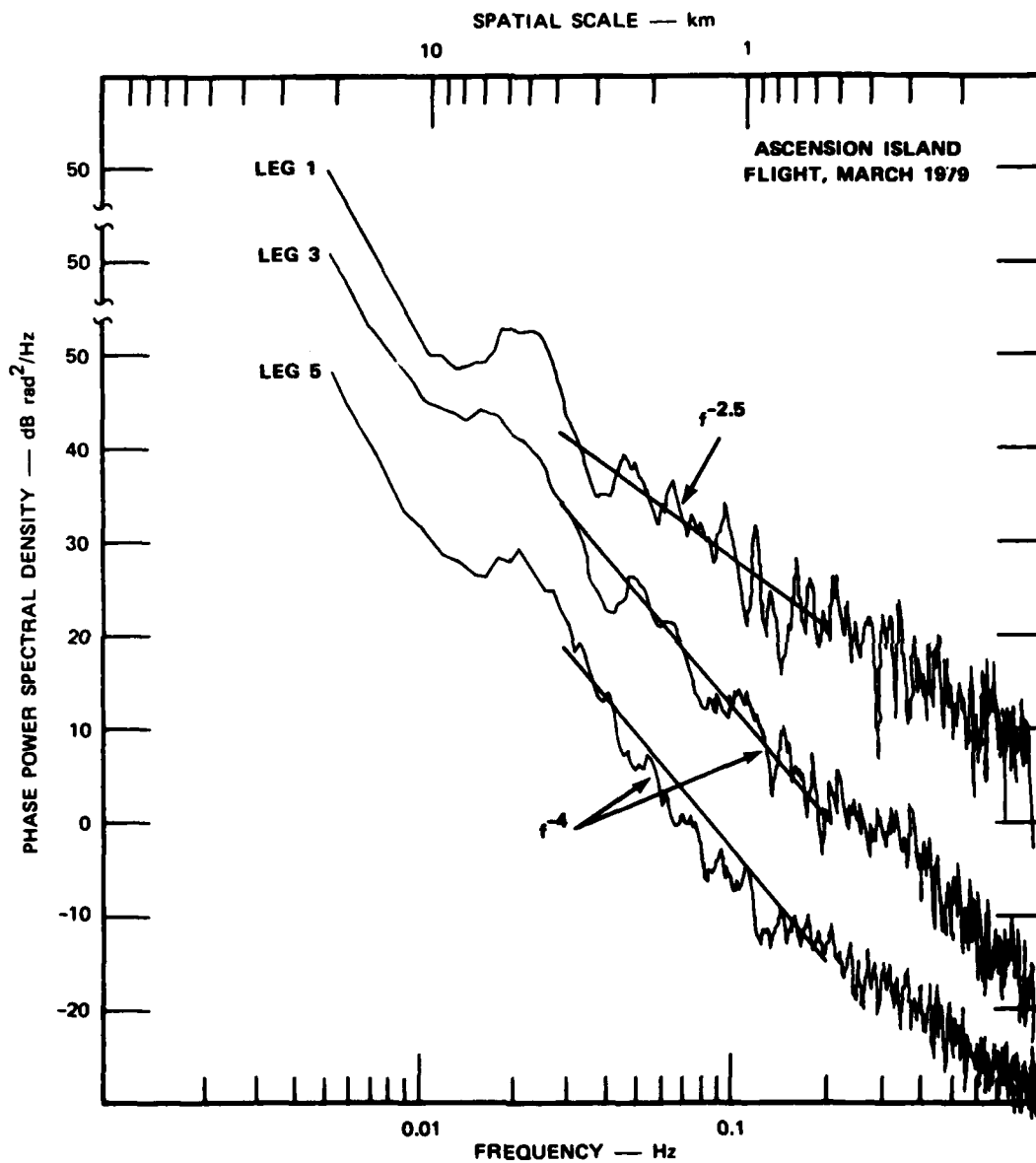


FIGURE 5 PHASE POWER SPECTRA FOR THE BUBBLE

At spatial scales larger than about 4 km, the spectra are nearly equal in shape and in energy content for all flight legs. The decay at the peak is only about 5 dB in 70 min. Because the scintillation technique is sensitive to  $(\Delta N)^2$  rather than  $(\Delta N/N)^2$ , however, some of the decrease may be caused by lower absolute plasma density. A detailed interpretation of the spectral features in this large-scale regime, which is dominated by aeronomic processes [Booker, 1979], is beyond the scope of this paper. The broad enhancement in energy centered near 7 km, which is made conspicuous by the energy depletion near 15 km, may be a remnant of the larger-scale perturbation (e.g., a gravity wave), which initiated the bubble. We note that this feature is very similar to that seen in the in situ electron density spectra presented by Kelley et al. [1982a].

Of more interest to the present study, and in contrast to the stability of large scale structure, that, at short scales decays rapidly during the observation period. For example, at an irregularity scale size near 1 km, the energy decays at an even rate of  $\sim 9$  dB per hour from Leg 1 to Leg 3 to Leg 5. Using the relationship

$$|\Delta N|^2(k, t_0 + \tau) = |\Delta N|^2(k, t_0) \exp - \{2k^2 D \tau\} \quad , \quad (1)$$

we find a diffusion coefficient for  $k = (2\pi/1000 \text{ m})$  of  $7 \text{ m}^2/\text{s}$ . On the other hand, the classical ambipolar cross-field diffusion coefficient (which is equal to twice the electron perpendicular diffusion coefficient) is given by

$$D_{\perp c} = 2\rho_e^2 v_e \approx 0.96 \text{ m}^2/\text{s} \quad . \quad (2)$$

The diffusion coefficient at the 1-km scale is thus considerably greater than the classical ambipolar rate.

As we discuss more fully below, an enhanced diffusion rate is not difficult to explain. What is more interesting is the fact that a single diffusion coefficient (independent of  $k$ ) cannot be used to describe the process. For example, by choosing  $D = 7 \text{ m}^2/\text{s}$ , we can match the decay

rate at 1 km, but that is the only scale at which the decay rate is matched by the classical formula given in Eq. (1). This result is illustrated in Figure 6 where Eq. (1) has been solved at a time,  $\tau_0$ , corresponding to Leg 5 with an input spectrum  $|\Delta N|^2(k, t_0)$  matched to the Leg 1 data (the straight line in Figure 6 is the least squares fit to the data in Leg 1). The solution matches the observed spectrum at 1 km. However, the experimental decay rate is considerably higher at longer wavelengths and considerably slower at shorter scales.

The data in Figure 5 provide an opportunity to determine empirically the scale-size dependance of the diffusion rate,  $D_\perp(k)$ . Over the scale-size regime  $400 \text{ m} < \lambda < 4 \text{ km}$ , the spectra in Figure 5 are nearly power law with slopes of -2.5, -4, and -5, respectively. By equating the value of  $|\Delta N|^2$  at 4 km for three such power law spectra and differencing the curves at all other scale sizes, we can solve Eq. (1) for  $D_\perp(k)$ . The result is plotted in Figure 7. The curve represents the average between differencing Leg 5 and Leg 1 and Leg 3 and Leg 1. The error bars indicate the differences in the two estimates. This empirical  $D_\perp(k)$ , of course, depends on the model in the sense that Eq. (3) assumes that each Fourier mode decays independently of the adjacent modes. As discussed below, it is unlikely that the physical mechanism or mechanisms that lead to the observed anomalous decay characteristics share the property of mode independence. The  $D_\perp(k)$  that we have found should thus be regarded as both empirical and model dependent.

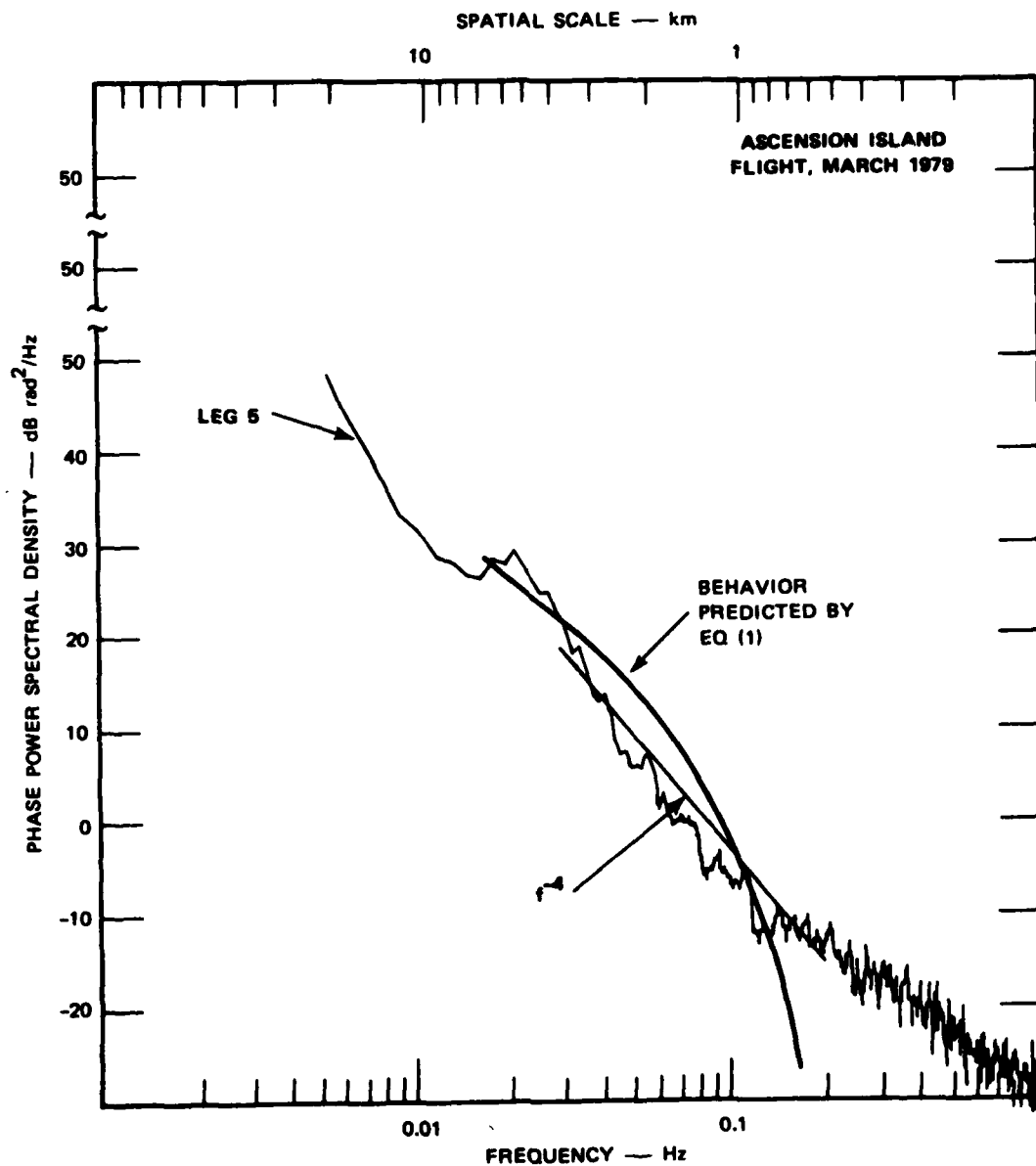


FIGURE 6 COMPARISON OF OBSERVATIONS OF THEORETICAL PREDICTIONS  
BASED ON EQ. (1)

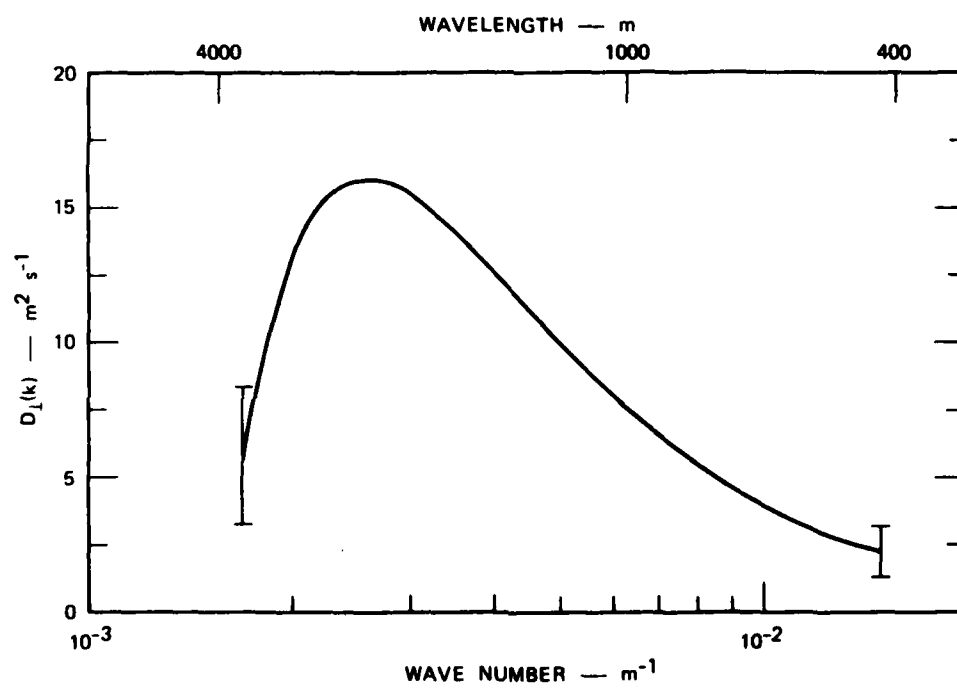


FIGURE 7 EMPIRICALLY DERIVED DIFFUSION COEFFICIENT

## V DISCUSSION

### A. Enhanced Classical Diffusion

A diffusion coefficient enhanced with respect to the ambipolar rate [Vickrey and Kelley, 1982] can be understood as follows. The ambipolar rate occurs when the more rapid perpendicular ion diffusion leads to a space-charge electric field that severely limits the ion flow and slightly enhances the electron velocity. An equilibrium results in which the two fluids diffuse at the same rate. Now if field-aligned currents can flow, for example, to a "conducting end plate" such as the E region in the auroral zone [Vickrey and Kelley, 1982], the ambipolar electric field can be "shorted out" and diffusion proceeds at the faster rate determined by

$$D_{\perp c} = \frac{\Sigma_1^F}{\Sigma_1^F + \Sigma_e^F + \Sigma_p^E} (D_{\perp e} - D_{\perp i}) + D_{\perp i} \quad (3)$$

where the  $\Sigma_p$  are the height-integrated Pedersen conductivities. The E region is of little importance in the nighttime equatorial zone. However, the conjugate F region has almost by definition a comparable height-integrated conductivity that, when substituted for  $\Sigma_p^E$  above, implies that  $D_{\perp c} \approx 0.5 D_{\perp i}$ . Taking  $v_{in} = 0.6 \text{ sec}^{-1}$  and  $\rho_1 = 5 \text{ m}$  corresponding to a height of 350 km yields  $D_{\perp c} = 7 \text{ m}^2/\text{s}$ . Thus, the enhanced diffusion rate is not as surprising as the observed wavelength dependence; i.e., the rate of diffusion could be explained classically, but the spectrum of decaying turbulence is another matter. In the next two sections, we investigate two mechanisms that produce diffusion whose rate depends on scale size.

## B. The Drift-Wave Hypothesis

Costa and Kelley [1978a,b], Burke et al. [1979], Huba and Ossakow [1981], Kelley [1982], and perhaps others have suggested that drift waves play an important role in F-region diffusion. In linear theories these waves are destabilized by gradients in the plasma and, in their nonlinear state, act to smooth out the gradients, which produce them. The result is anomalous diffusion of the driving structure.

Gary [1980] has analytically studied anomalous diffusion due to drift waves. The waves grow at wavelengths such that  $k_{\perp} \rho_i \gg 1$ , which corresponds to wavelengths below about 40 m. Kelley et al. [1982b] and Kelley [1982] have compared the amplitude and spectral forms of both density and electric field fluctuations predicted by Gary [1980] and by Bernhardt et al. [1982] in this wavelength regime, and found excellent agreement with data obtained in the topside equatorial spread F environment (i.e., altitudes  $> 280$  km).

Gary's analytical form for the anomalous diffusion coefficient is

$$D_a = \frac{\pi}{9} \left( \frac{KT}{M} \right)^{3/2} \left( \frac{1}{\Omega i} \right)^2 \left( \frac{1}{n} \frac{dn}{dx} \right) \quad (4)$$

which can also be written

$$D_a = 1.29 D_{\perp i} (Kl) \quad (5)$$

where  $l$  is the ion mean free path parallel to the magnetic field,  $(V_{in}/v_{in})$ , and  $K$  is the gradient scale-length,  $(1/n \, dn/dx)^{-1}$ , wave number of the driving scale. For a sinusoidal driver with wavelength of 3 km, corresponding to the break in the spectrum and a mean free path of 450 m,  $D_a = 1.2 D_{\perp i} \approx 17 \, \text{m}^2/\text{s}$ .

This result is in reasonable agreement with the present data set in the sense that the enhanced decay at long wavelengths may be explained. Because the drift waves themselves only occur at very short wavelengths, however, one must hypothesize a link in  $k$  space for this mechanism to be

valid. In fluid turbulence theory, such a linkage occurs in the inertial subrange where energy is passed between adjacent wave numbers, leading to a cascade from large to small scales. The net effect is to maintain the energy level in the intermediate range, with dissipation occurring at short wavelengths.

These arguments must remain somewhat speculative because turbulence theory is not as well developed in plasma applications. The data are not inconsistent with these concepts, however, provided an analog of the inertial subrange exists in plasmas.

### C. The Image Formation Process

An alternative mechanism that produces a scale size dependent loss of F-layer structure has been proposed by Vickrey et al. [1984], who have investigated the formation of image striations in the E layer theoretically. Images result from the finite compressibility of the E-region ion gas. Because the electron gas is incompressible in both the E and F regions, however, the image formation process redistributes electrons along the magnetic field line such that  $\nabla \cdot J \equiv 0$ .

The model calculations of Vickrey et al. [1984], show that the saturated E region image spectrum has a peak near 1 km and scale size in agreement with near-equatorial rocket observations. Because the image irregularities grow at the expense of F layer plasma, Vickrey et al. [1984], argued that the "effective" diffusion rate in the F layer would reflect, at least qualitatively, the scale-size dependence of the image formation process. The present observations support that argument. It should be kept in mind, however, that the observed spectrum is a balance between possibly scale-size dependent drivers and loss mechanisms. Nevertheless, the present observations support a "nondriven" situation in which the spectral evolution is determined purely by diffusion processes. A quantitative time-dependent cross-field diffusion model including magnetic field-line coupling effects is currently being developed and will be reported elsewhere.



## VI SUMMARY

We have shown unique airborne observations of the spectral evolution of ionospheric structure in an isolated, decaying plasma bubble. The temporal behavior of the decaying plume structure suggests that the loss mechanism of structure is scale-size dependent. The effective cross-field diffusion rate deduced from the observations is scale-size dependent and in qualitative agreement with the theoretical model described by Vickrey et al. [1984].

## REFERENCES

- Bernhardt, P. A., M. B. Pongratz, S. Peter Gary, and M. F. Thomsen, "Dissipation of Ionospheric Irregularities by Wave-Particle and Collisional Interactions," J. Geophys. Res., 87(A4), 2356-2362, April 1, 1982.
- Booker, H. G., "The Role of Acoustic Gravity Waves in the Generation of Spread F and Ionospheric Scintillations," J. Atmos. Terr. Phys., 41, 501, 1979.
- Burke, W. J., D. E. Donatelli, R. C. Sagalyn, and M. C. Kelley, "Low Density Regions Observed at High Altitudes and their Connection with Equatorial Spread F," Planet. Space Sci., 27, 593, 1979.
- Costa, E., and M. C. Kelley, "On the Role of Steepened Structures and Drift Waves in Equatorial Spread F," J. Geophys. Res., 83, 4359, 1978a.
- Costa, E., and M. C. Kelley, "Linear Theory for the Collisionless Drift Wave Instability with Wavelengths near the Ion Gyroradius," J. Geophys. Res., 83, 4365, 1978b.
- Gary, S. P., "Waveparticle Transport from Electrostatic Instabilities," Phys. Fluids., 23, 1193, 1980.
- Huba, J. D. and S. L. Ossakow, "Diffusion of Small-Scale Density Irregularities During Equatorial Spread F," J. Geophys. Res., 86., 9107, 1981.
- Kelley, M. C., "Nonlinear Saturation Spectra of Electric Fields and Density Fluctuations in Drift Wave Turbulence," Phys. Fluids., 25(6), 1002, June 1982.
- Kelley, M. C., R. C. Livingston, C. L. Rino, and R. T. Tsunoda, "The Vertical Wave Number Spectrum of Topside Equatorial Spread F: Estimates of Backscatter Levels and Implications for a Unified Theory," J. Geophys. Res., 87(A7), 5217-5221, July 1, 1982a.
- Kelley, M. C., R. Pfaff, K. D. Baker, J. C. Ulwick, R. Livingston, C. Rino, and R. Tsunoda, "Simultaneous Rocket Probe and Radar Measurements of Equatorial Spread F--Transitional and Short Wavelength Results," J. Geophys. Res., 87, 1575, 1982b.
- Livingston, R. C., "Heater-Generated Intermediate-Scale Irregularities: Spatial Distribution and Spectral Characteristics," Radio Sci., 18, 253, 1983.

# REFERENCES (concluded)

- Livingston, R. C., C. L. Rino, J. P. McClure, and W. B. Hanson, "Spectral Characteristics of Medium-Scale Equatorial F-Region Irregularities," J. Geophys. Res., 86, 2421, 1981.
- Ossakow, S. L., "Ionospheric Irregularities," Rev. Geophys. Space Phys., 17, 521, 1979.
- Rino, C. L., "A Power Law Phase Screen Model for Ionospheric Scintillation Studies, 1. Weak Scatter," Radio Sci., 14, 1135, 1979.
- Tsunoda, R. T., "Time Evolution and Dynamics of Equatorial Backscatter Plumes, 1. Growth Phase," J. Geophys. Res., 86, 139, 1981.
- Vickrey, J. F., M. C. Kelley, R. Pfaff and S. R. Goldman, "Low-Altitude Image Striations Associated with Bottomside Equatorial Spread F: Observations and Theory," J. Geophys. Res., 89(A5), 2955-2961, 1984.
- Vickrey, J. F. and M. C. Kelley, "The Effects of a Conducting E Layer on Classical F Region Cross-Field Plasma Diffusion," J. Geophys. Res., 87, 4461, 1982.
- Weber, E. J., J. Buchau, and J. G. Moore, "Airborne Studies of Equatorial F Layer Ionospheric Irregularities," J. Geophys. Res., 85, 4631, 1980.

END

FILMED

10-84

DTIC